Supplementary Information for

Structure of the mannose transporter of the bacterial phosphotransferase system

Xueli Liu[1], Jianwei Zeng[1], Kai Huang[1], Jiawei Wang[1]

[1]State Key Laboratory of Membrane Biology, Beijing Advanced Innovation Center for Structural Biology, School of Life Sciences, Tsinghua University, Beijing 100084, China

Correspondence: Jiawei Wang

Email: jwwang@tsinghua.edu.cn

Materials and methods

Overexpression and purification of the ManYZ complex

Overexpression of ManYZ was induced in *E. coli* knock out BL21(DE3) by 0.2 mM isopropyl b-D-thiogalactoside (IPTG) when the cell density reached a D_{600} of 1.5. After growth overnight at 4 ℃, the cells were harvested, homogenized in buffer containing 25 mM Tris-HCl pH 8.0 and 150 mM NaCl, and disrupted by sonication. Cell debris was removed by low-speed centrifugation for 10 min. The supernatant was applied to ultracentrifugation at 150,000 g for 1 h. The membrane pellets were collected and homogenized in the buffer (25 mM Tris pH 8.0, 150 mM NaCl and 2mM Mannose), and then solubilized with 2% (w/v) n-dodecyl-b-D-maltoside (DDM, Anatrace) at 4 ℃for 2 h. The insoluble fraction was precipitated by ultracentrifugation (150,000 g) for 30 min at 4 ℃. The supernatant was incubated with Ni-NTA resin (Qiagen) for an additional 30 min at 4 ℃. The resin was then rinsed with the buffer containing 25 mM Tris pH 8.0, 150 mM NaCl, 2 mM mannose, 20 mM imidazole, and 0.02% DDM three times. The protein was eluted with the washing buffer plus 250 mM imidazole and further concentrated to 2 mL, then the protein was applied to Superdex 200 10/300 GL (SD200, GE Healthcare) pre-equilibrated with buffer containing 25 mM Tris pH 8.0, 150 mM NaCl, 2 mM mannose and 0.07% digitonin. Peak fractions were collected. Purified ManYZ at a concentration of approximately 10 mg/ml were placed on glow-discharged holey carbon grids (Quantifoil Cu 300 mesh, R1.2/1.3). The grids were blotted, and flash-frozen in liquid ethane cooled by liquid nitrogen using FEI Vitrobot Mark IV at 8°C and 100% humidity. All set grids were retained in liquid nitrogen until data collection.

Cryo-EM data acquisition

The grids with optimal ice thickness and particle density were transferred to a Titan Krios TEM operated at 300 kV and equipped with Gatan GIF Quantum energy filter and Gatan K2 direct electron detector. A total of 9847 movie stacks were automatically collected using AutoEMation II (developed by Jianlin Lei) [1] in the super-resolution mode with 20-eV slit in energy filter at a nominal magnification of 105,000× with defocus range from −1.5 to −2.9 μm. Each micrograph stack, which contained 32 frames, was exposed for 8.0 s with a total electron dose of ~50 e−/Å^2. The stacks were motion corrected using MotionCor2 [2] with a binning factor of 2, resulting in a pixel size of 1.338 Å. Dose weighting was performed concurrently [3]. Gctf [4] was used to estimate the defocus values.

Cryo-EM image processing

The particles were automatically picked with Gautomatch (developed by Kai Zhang, https://www.mrc-lmb.cam.ac.uk/kzhang/Gautomatch/). After 2D classification with RELION 1.4 or 2.0[5,6], 3,272,777 particles were selected and subjected to global angular search 3D classification using RELION 2.0 with one class and step size of 7.5˚, and then to 3D classification with 4 classes. Each class was subjected to 3D sub-classification with 4 classes again with step size of 7.5˚. After several rounds of 3D sub-classification, a C3 symmetry-like map was obtained. 3,272,777 particles which selected from 2D classification were subjected to 3D classification again and used the C3 symmetry-like map as the reference. A resulting good map was chosen and subjected to further 3D classification with C3 symmetry. The new resulting C3 symmetry map was used as reference for local angular search 3D classification with 3-10 classes, and local search range of 15°. A total of 716,734 good particles were combined and subjected to further 3D classification, from which 325,142 good particles were selected and subjected to 3D auto-refinement with C3 symmetry, resulting in a final resolution at 4.24 Å with traceable densities in the TM region. A mask on $ManY_3$:$ManZ_3$ (IIC_3:IID_3) was applied, resulting in a final resolution at 3.52 Å. The resolution was estimated with the gold-standard Fourier shell correlation 0.143 criterion[7] with high resolution noise substitution[8]. Local resolution variations were estimated using ResMap[9].

Model Building and structure refinement

The 3.52 Å ManYZ reconstruction map was used for *de novo* model building in EMBuilder[10], and adjusted manually in COOT[11]. In total, 245 residues of ManY (4-248) and 266 residues of ManZ (17-282) are structurally modeled and assigned reliably. Structure refinements were carried out by PHENIX in real space with secondary structure and geometry restraints to prevent structure overfitting[12]. Statistics of 3D reconstruction and model refinement can be found in Table S1. All structure figures were prepared using PyMol[13].

Counterflow assay

Liposomes were prepared as described previously[14]. For each assay, 5 μL of concentrated proteoliposomes (ManYZ or mutations) were added into 94 μL KPM

7.5 buffer plus 1 μCi D-[2-^{3}H] mannose (specific radioactivity 17.8 Ci mmol^{-1}, PerkinElmer) and 0.01 mM cold mannose. The final concentration of the external D-[2-^{3}H] mannose was 0.6 μM. The uptake of radiolabelled substrates was stopped at 15 min by rapidly filtering the solution through 0.22 mm filters (Millipore). The filter membranes were washed with 2 ml ice-cold KPM 7.5 buffer immediately, solubilized with 0.5 ml Optiphase HISAFE 3 (PerkinElmer) and used for liquid scintillation counting with MicroBeta JET (PerkinElmer). Liposomes without protein were tested as a negative control. All counter-flow assays were performed at 25 ℃ and repeated at least three times. Error bars represent s.e.m.

Supplementary Figures and Legends

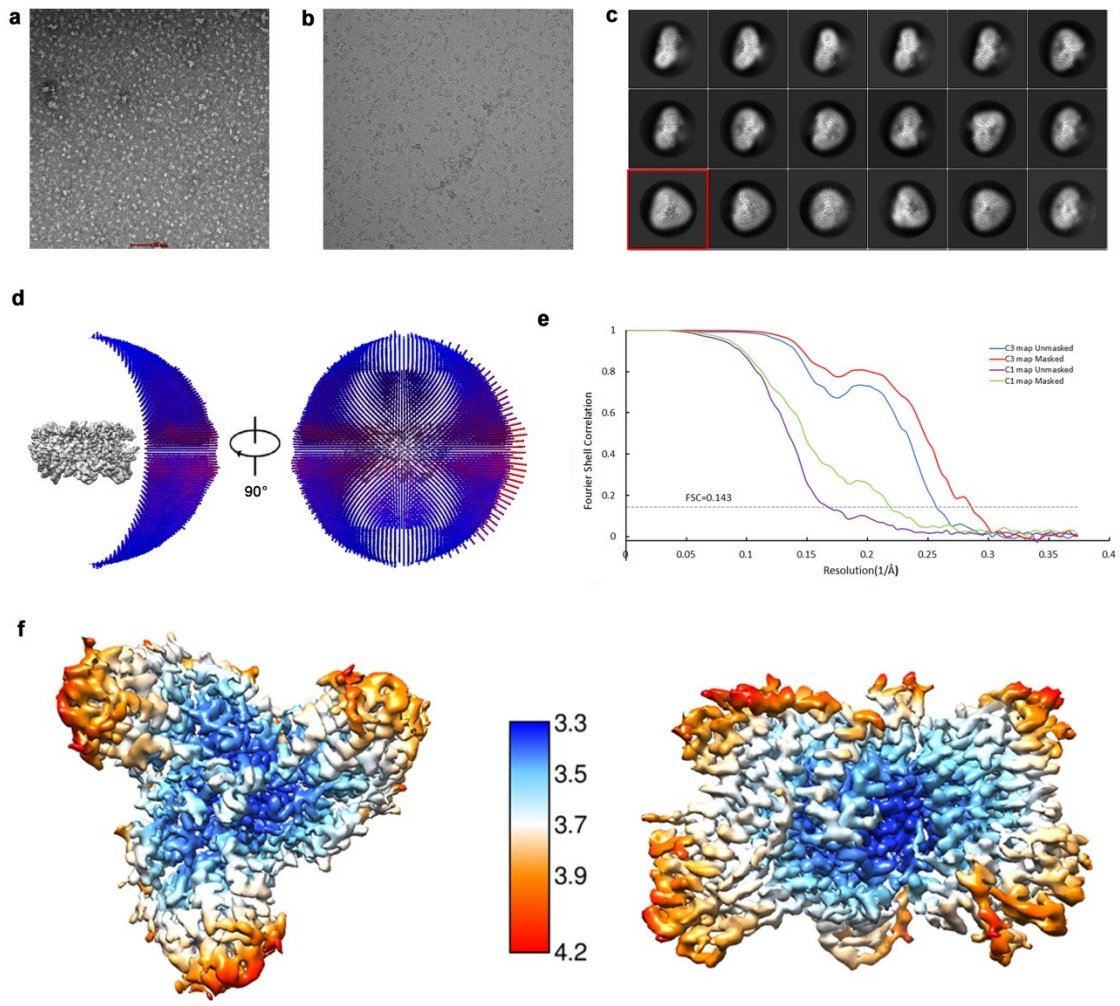

Supplementary information, Fig. S1 Cryo-EM analysis of the ManYZ complex.

(a) A representative negative-stain raw micrograph of ManYZ. (b) A representative cryo-EM raw micrograph of ManYZ. (c) Representative cryo-EM 2D class averages of the complex. Top view of trimer is indicated with a red box. (d) Angular distribution of cryo-EM particles used for final structural refinement. (e) FSC curve (gold-standard FSC) as a function of resolution for C1 and C3 symmetries, before and after mask application. (f) Local resolution maps of ManYZ calculated by ResMap[9].

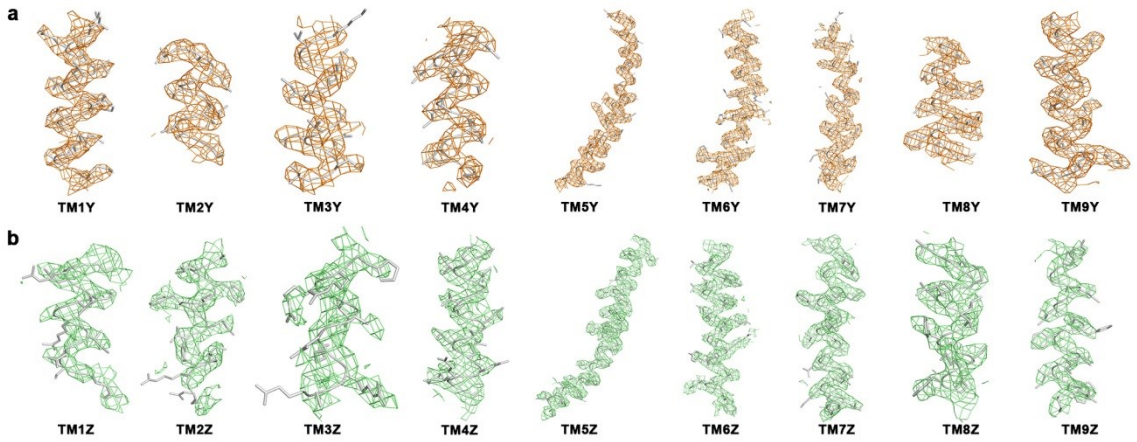

Supplementary information, Fig. S2 Electron microscopy density of different portions of the transmembrane helices at 5σ level.

(a) ManY: TM1-9Y. (b) ManZ: TM1-9Z.

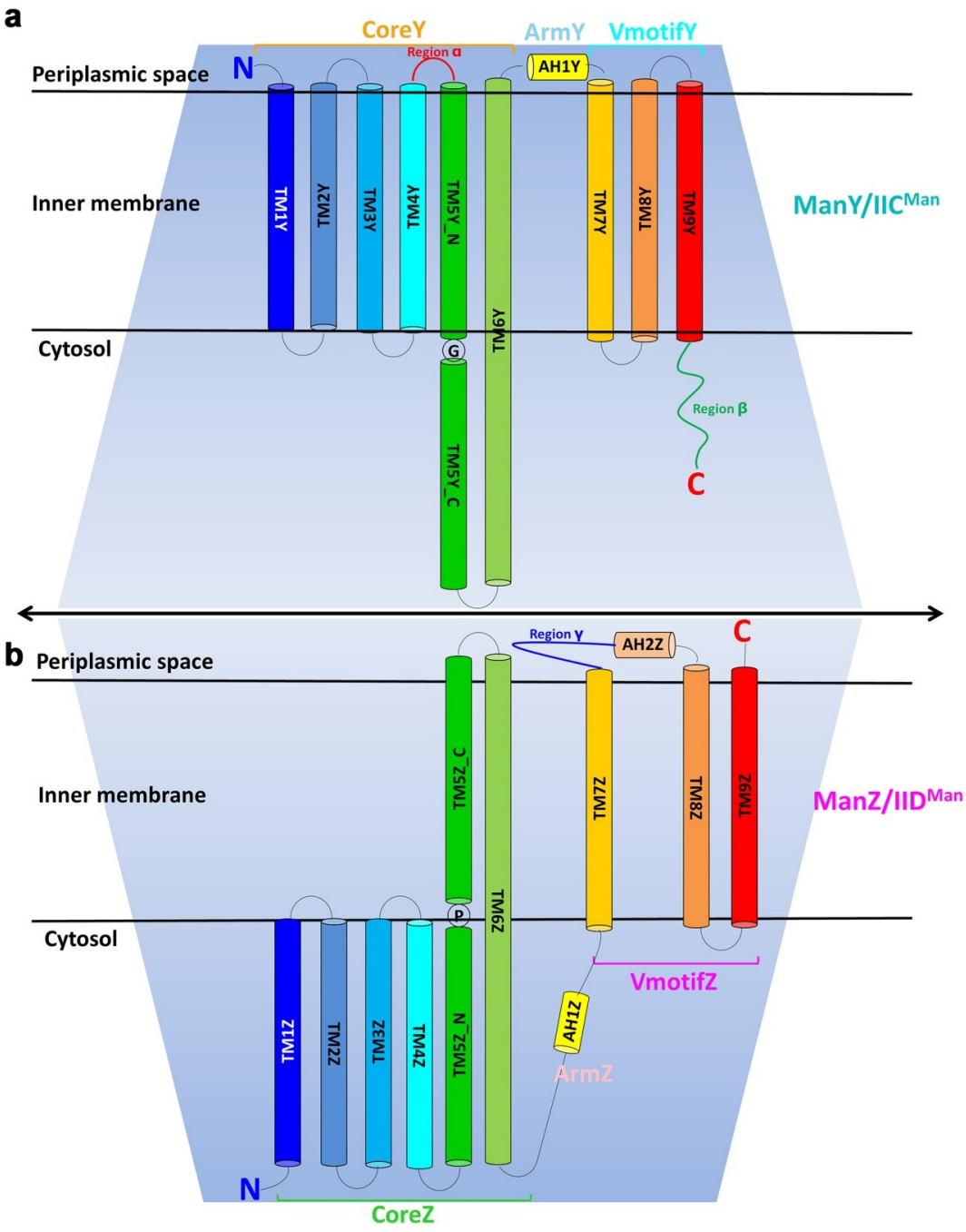

Supplementary information, Fig. S2 Topology diagram of ManYZ.

The helices are denoted as cylinders and rainbow-colored. The diagram is oriented with the extracellular side on top. The black lines show the approximate location of the membrane, and the N- and C-termini are labelled. The ManYZ structural symmetries are highlighted by the trapezoids, which emphasize their relative orientation. The TM segments comprising the transporter Core are denoted as “CoreY” and “CoreZ”, while those comprising the Vmotif are denoted as “VmotifY” and “VmotifZ”, respectively. (a) ManY and (b) ManZ.

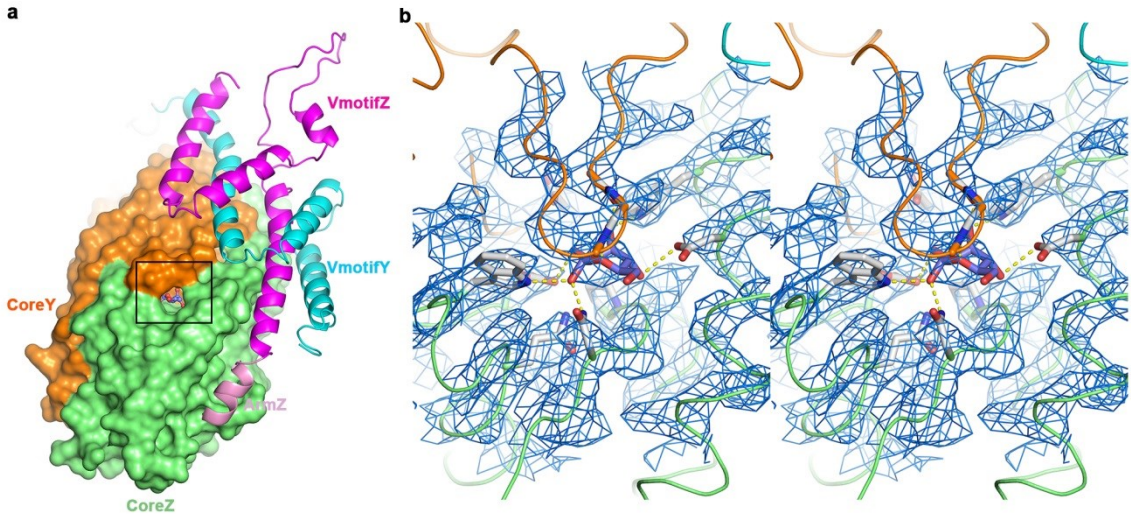

Supplementary information, Fig. S4 Substrate-binding site.

(a) Surface representation of Core domain, and cartoon representation of Vmotif domain. (b) Stereoview of the cryo-EM map around the substrate-binding site.

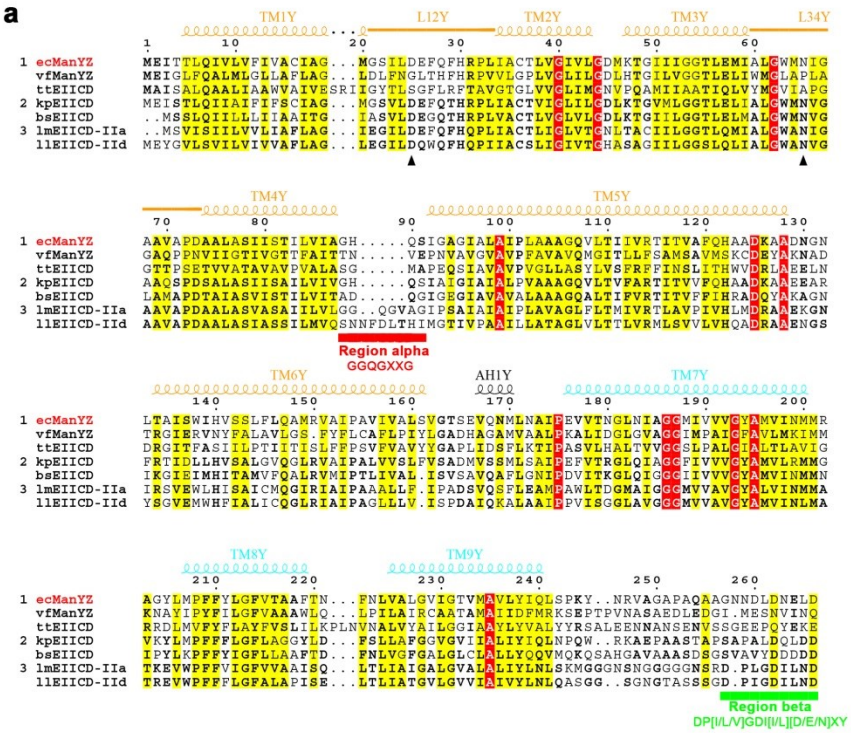
a
TM1Y
L12Y
TM2Y
TM3Y
L34Y
TM4Y
TM5Y
Region alpha
GGQGXXG
TM6Y
AH1Y
TM7Y
TM8Y
TM9Y
Region beta
DP[I/L/V]GDI[I/L][D/E/N]XY
b
TM1Z
L12Z
TM2Z
TM3Z
L34Z
TM4Z
TM5Z
TM6Z
AH1Z
TM7Z
AH2Z
Region gamma
TM8Z
TM9Z

Supplementary information, Fig. S5 Sequence alignment of *E. coli* ManY and ManZ with homologs from other species and organisms.

The listed ManYZ homologs include ManYZ from *E. coli (ec), V. furnissii (vf), T. tengcongensis (tt), K. pneumoniae (kp), B. subtilis (bs), Listeria monocytogenes (lm), and Lactococcus lactis (ll).* ttIIC and ttIID are linked as a single chain. vfManYZ is inactive with GlcNAc and Fru[15]. ecManYZ and bsEIICD support bacteriophage lambda infection, while kpEIICD does not. lmEIICD is the receptor of class IIa bacteriocin (such as pediocin PA-1), and llEIICD for class IId (such as lactococcin A). Three sequence regions (α, β, γ) that distinguish members of the bacteriocin-susceptible group I from the other groups, together with the corresponding motifs, are indicated below the sequence alignment, while secondary structural elements are indicated above the sequence alignment. The substrate binding residues are indicated with black cycles. The sequences were aligned with ClustalW[16]. (a) ManY alignment. (b) ManZ alignment.

Supplementary information, Table S1 Statistics and model refinement.

	$ManY_3$:$ManZ_3$ complex
Data collection	
EM equipment	Titan Krios (Thermo Fisher)
Voltage (kV)	300
Detector	Gatan K2 Summit
Energy filter	Gatan GIF Quantum, 20 eV
Pixel size (Å)	1.338
Electron dose ($e^-/Å^2$)	50
Defocus range (μm)	-1.5 ~ -2.9
Reconstruction	
Software	RELION 1.4 & 2.0[5,6]
Number of used particles	309,996
Symmetry	C3
Final masked resolution (Å)	3.52
Final unmasked resolution (Å)	3.93
Map sharpening B-factor ($Å^2$)	-188
Model building	
Software	EMBuilder[10] & Coot[17]
Refinement	
Software	Phenix.real_space_refine[12]
Validation	
EMRinger score	2.13
R.m.s. deviations	
Bond length (Å)	0.008
Bond angle (°)	1.63
Ramachandran plot statistics (%)	
favored	87.44
Outlier	0.0
Rotamer outliers (%)	1.0
Clashscore	6.99

References

1 Lei, J. & Frank, J. Automated acquisition of cryo-electron micrographs for single particle reconstruction on an FEI Tecnai electron microscope. *J Struct Biol* **150**, 69-80, doi:10.1016/j.jsb.2005.01.002 (2005).

2 Zheng, S. Q. *et al.* MotionCor2: anisotropic correction of beam-induced motion for improved cryo-electron microscopy. *Nat Methods* **14**, 331-332, doi:10.1038/nmeth.4193 (2017).

3 Grant, T. & Grigorieff, N. Measuring the optimal exposure for single particle cryo-EM using a 2.6 A reconstruction of rotavirus VP6. *Elife* **4**, e06980, doi:10.7554/eLife.06980 (2015).

4 Zhang, K. Gctf: Real-time CTF determination and correction. *J Struct Biol* **193**, 1-12, doi:10.1016/j.jsb.2015.11.003 (2016).

5 Scheres, S. H. Semi-automated selection of cryo-EM particles in RELION-1.3. *J Struct Biol* **189**, 114-122, doi:10.1016/j.jsb.2014.11.010 (2015).

6 Kimanius, D., Forsberg, B. O., Scheres, S. H. & Lindahl, E. Accelerated cryo-EM structure determination with parallelisation using GPUs in RELION-2. *eLife* **5**, doi:10.7554/eLife.18722 (2016).

7 Rosenthal, P. B. & Henderson, R. Optimal determination of particle orientation, absolute hand, and contrast loss in single-particle electron cryomicroscopy. *J Mol Biol* **333**, 721-745 (2003).

8 Chen, S. *et al.* High-resolution noise substitution to measure overfitting and validate resolution in 3D structure determination by single particle electron cryomicroscopy. *Ultramicroscopy* **135**, 24-35, doi:10.1016/j.ultramic.2013.06.004 (2013).

9 Kucukelbir, A., Sigworth, F. J. & Tagare, H. D. Quantifying the local resolution of cryo-EM density maps. *Nature methods* **11**, 63-65, doi:10.1038/nmeth.2727 (2014).

10 Zhou, N., Wang, H. & Wang, J. EMBuilder: A Template Matching-based Automatic Model-building Program for High-resolution Cryo-Electron Microscopy Maps. *Scientific reports* **7**, 2664, doi:10.1038/s41598-017-02725-w (2017).

11 Emsley, P., Lohkamp, B., Scott, W. G. & Cowtan, K. Features and development of Coot. *Acta Crystallogr D Biol Crystallogr* **66**, 486-501, doi:10.1107/S0907444910007493 (2010).

12 Afonine, P. V. *et al.* Real-space refinement in PHENIX for cryo-EM and crystallography. *Acta crystallographica. Section D, Structural biology* **74**, 531-544, doi:10.1107/s2059798318006551 (2018).

13 DeLano, W. L. The PyMOL Molecular Graphics System. *on World Wide Web http://www.pymol.org* (2002).

14 Sun, L. *et al.* Crystal structure of a bacterial homologue of glucose transporters GLUT1-4. *Nature* **490**, 361-366, doi:10.1038/nature11524 (2012).

15 Bouma, C. L. & Roseman, S. Sugar transport by the marine chitinolytic bacterium Vibrio furnissii. Molecular cloning and analysis of the mannose/glucose permease. *The Journal of biological chemistry* **271**, 33468-33475 (1996).

16 Thompson, J. D., Gibson, T. & Higgins, D. G. Multiple sequence alignment using ClustalW and ClustalX. *Current protocols in bioinformatics*, 2.3. 1-2.3. 22 (2002).

17 Emsley, P. & Cowtan, K. Coot: model-building tools for molecular graphics. *Acta crystallographica. Section D, Biological crystallography* **60**, 2126-2132, doi:10.1107/s0907444904019158 (2004).